SAND2017-5460C

Proceedings of ASME 2017 Fluids Engineering Division Summer Meeting
FEDSM2017
July 30-August 3, 2017, Waikoloa, USA

FEDSM2017-69378

A CONFORMAL DECOMPOSITION FINITE ELEMENT METHOD FOR DYNAMIC WETTING APPLICATIONS

David R. Noble*
Fluid and Reactive Processes
Sandia National Laboratories
Albuquerque, New Mexico 87185
Email: drnoble@sandia.gov

Alec Kucala
Fluid and Reactive Processes
Sandia National Laboratories
Albuquerque, New Mexico 87185
akucala@sandia.gov

Mario J. Martinez
Fluid and Reactive Processes
Sandia National Laboratories
Albuquerque, New Mexico 87185
mjmarti@sandia.gov

ABSTRACT

An enriched finite element method is described for capillary hydrodynamics including dynamic wetting. The method is enriched via the Conformal Decomposition Finite Element Method (CDFEM). Two formulations are described, one with first-order accuracy and one with second-order accuracy in time. Both formulations utilize a semi-implicit form for the surface tension that is shown to effectively circumvent the explicit capillary time step limit. Sharp interface boundary conditions are developed for capturing the dynamic contact angle as the fluid interface moves along the wall. By virtue of the CDFEM, the contact line is free to move without risk of mesh tangling, but is sharply captured. Multiple problems are used to demonstrate the effectiveness of the methods.

1. INTRODUCTION

Accurate models of capillary hydrodynamics and dynamic contact lines are important in many industrial technologies including coatings, microfluidics, and subsurface geosciences (e.g., enhanced oil recovery, geologic carbon storage).

Dynamic wetting, or simply wetting, refers to the displacement of one fluid by another, for example gas displaced by water, along a solid surface. The fluids are immiscible, and a surface tension, σ, is exerted along their common interface. In the absence of motion, the fluid interface contacts the solid surface at the equilibrium or static wetting angle, θ_s. With motion, the apparent, macroscopically observed dynamic contact angle, θ_d differs from the equilibrium wetting angle. As discussed by [1, 2], among others, dynamic wetting operates at multiple scales, and the aforementioned angles are referred to as macroscopic (i.e. visible) angles. Theoretical models for this three-phase moving contact line (MCL) problem are further complicated by the singularity implied by the paradox of the typically applied no-slip condition on the solid surface in the vicinity of the moving contact line. Two types of models have been posed to explain dynamic contact, hydrodynamic models as exemplified by [1, 3, 4] and a molecular-based model [5, 6]. These theories give the relationship between velocity of the contact line and the dynamic wetting angle.

A widely-applied model is based on using a Navier slip condition with either a prescribed constant contact angle, or improved by imposing a theoretical relation between contact line speed and dynamic contact angle. The slip model regularizes the stress singularity at the MCL. This type of MCL model has been applied with both volume-of-fluid (VOF) methods, e.g., [7, 8] and Level Set methods, e.g., [9, 10]. Cahn-Hilliard phase field methods [11] have also been applied. It is worthwhile to note that these types of methods approximate the fluid interface in a diffuse manner.

This paper introduces a new numerical implementation for describing dynamic contact lines. The method is based on a weak form specification of the balance of surface forces at the contact line combined with a level set for tracking the fluid interface. The force balance only weakly enforces the equilibrium contact angle, instead producing a dynamic contact angle resulting from a natural balance of forces at the contact line. Similar models

*Address all correspondence to this author.

have recently appeared for steady [12] and dynamic [13] MCLs. In contrast, our method dynamically tracks a sharp fluid interface allowing a more accurate integral representation of capillary forces.

The sharp interface method is based on the Conformal Decomposition Finite Element Method (CDFEM), which is an enriched finite element method that is able to describe arbitrarily discontinuous physics across moving interfaces. The method was developed at Sandia National Laboratories to simulate multiphase and multimaterial problems with dynamic topology using a finite element code that was originally designed for problems with static topology. The location of the moving interface is described using a level set. Nodes are added at the intersection of the level set surface with the edges of the input mesh, and a conforming mesh is generated automatically. Standard unstructured mesh data structures are generated for the resulting conformal mesh in terms of element blocks and side sets. This general framework allows the physics code to describe either weak or strong discontinuities across the interface using standard finite element methods.

For enriched finite element methods, careful attention must be given to the time integration, particularly in regard to the enriched degrees of freedom that are dynamically associated with the moving interfaces. Recent work has shown dynamic CDFEM with second-order accuracy in space and time for moving interface problems with both strong and weak discontinuities [14]. These methods are further developed for the solution of the Navier-Stokes equations for dynamic wetting applications here. The finite element formulation for the Navier-Stokes equations, capillary condition, and wetting conditions has a great deal in common with the Arbitrary Lagrangian Eulerian (ALE) methods presented in [13]. The proposed method is verified using numerical simulations of problems with analytical solutions. The method is validated by comparison with the results of wetting experiments.

2. METHODOLOGY

Conformal Decomposition Finite Element Method

In CDFEM, the finite element approximation space is enriched by decomposing the finite elements that are crossed by the zero level set into elements that simulataneously conform to the original element and the zero level set surface. The input mesh is composed of linear triangular elments in two dimensions (2D) or linear tetrahedral elements in three dimensions (3D). As a result, the interface consists of line segments in 2D, and triangles in 3D. The decomposition algorithm, including degeneracy handling, is described in [15]. The result of the decomposition is a fully connected finite element mesh that conforms to the instantaneous fluid domains. The conformal decomposition algorithm is much like element refinement for non-conformal adaptivity. The elements are subdivided into new elements and nodes are added in the process, and field data at newly added nodes are populated, or prolonged, using existing field data. Unlike nonconformal adaptivity, however, the new elements conform to the moving fluid domains, and the added nodes lie on the interfaces between the fluids.

Moving Mesh Approach for Dynamic CDFEM.

The issue of prolongation in CDFEM was covered extensively in [14]. Fields that contain weak discontinuities, such as velocity in multiphase flows, or strong discontinuities, such as pressure in multiphase flows, require a prolongation method that accounts for these discontinuities. Due to interfacial motion, some nodes of the background mesh will change material as the interface passes over them. Discontinuous fields at these nodes must be repopulated to account for the change in material. In the current work, the moving mesh approach that was developed in [14] is used to handle the dynamic discretization for velocity and pressure. The level set field is prolonged using simple interterpolation since the field is continuous. The newly created nodes on the interface and nodes that have changed material are considered to have moved to their current location from a previous location where the velocity and pressure were already defined. The remaining nodes are taken to be stationary. This fictitious mesh motion is accounted for by a mesh velocity correction in the advection term of the Navier-Stokes equations. In this way, the momentum equation is modified to handle the dynamic discretization as the interface evolves. A subtle, but important, consequence of using the moving mesh approach for the dynamic discretization is that the transport equations must be solved after the conformal decomposition is performed in order to accurately account for the interface motion. A typical algorithm involves solving for the new fluid domain locations, decomposing the mesh to conform to the new domains, and solving the transport physics on the new domains, including the mesh motion term to account for the change in domain.

Semi-implicit Finite Element Methods for Capillary Hydrodynamics

It is common for level set methods for capillary hydrodynamics to use explicit time integration. The Navier-Stokes equations are solved using the level set field from the previous time plane and then the level set equation is solved using the resulting velocity field. These implementations are first-order accurate in time and subject to a stringent time step restriction:

$$\Delta t \leq \sqrt{\frac{\rho \Delta x^3}{2\pi\sigma}}. \tag{1}$$

In order to circumvent this restriction, a semi-implicit method was proposed that includes the impact of the evolving level set

field in the Navier-Stokes equations [16]. In this case, the Navier-Stokes equations are solved using the old level set values, but a semi-implicit term is added that accounts for the impact of the evolving level set field on the velocity. This term involves interface diffusion and stabilizes the system of equations, circumventing the explicit time step limit. The semi-implicit time integration has the added benefit of improving the time accuracy of the method. In order to take advantage of the improved accuracy, the Navier-Stokes equations must be solved with the semi-implicit term to account for the evolving level set field. The the level set equation is solved using the updated velocity. Note that this ordering is in conflict with the requirements for the moving mesh approach for the evolving discretization. Two approaches are proposed to work around this issue. A first-order accurate method in time is proposed that reorders the steps to meet the requirements for the moving mesh approach. This approach accepts an error proportional to the time step size because of this order. A second-order method is also proposed using a predictor-corrector algorithm that meets the requirements for both the moving mesh approach and semi-implicit method, and consequently recovers second-order accuracy in space and time. However, the method requires two Navier-Stokes solves per time step.

First-order Accurate CDFEM for Capillary Hydrodynamics

First-order temporal accuracy can be obtained by the following proposed algorithm:

1. Solve level set equation using the old velocity
2. Perform conformal decomposition, creating the domain Ω^{n+1}
3. Solve the Navier-Stokes equations using the moving mesh term and semi-implicit term

In this case, a semi-implicit term is used as a stabilization term along the lines of [17]. The impact of using this term in this way is that the method is only first-order accurate in time. Consistent with this order of accuracy, backward Euler time integration is used.

Second-order Accurate, Semi-implicit CDFEM for Capillary Hydrodynamics

Second-order temporal accuracy can be obtained by the following proposed algorithm:

1. Navier-Stokes predictor: Solve the Navier-Stokes equations using semi-implicit term with old interface location for the predicted velocity, $\tilde{\mathbf{u}}$
2. Solve level set equation using predicted velocity
3. Perform conformal decomposition, creating the domain Ω^{n+1}
4. Navier-Stokes corrector: Solve the Navier-Stokes equations using the moving mesh term and semi-implicit term, now based on the velocity correction

Here, a semi-implicit term in the momentum predictor is used to incorporate the effect of the moving interface, since the integration conforms to the older interface location. After updating the level set field using the predicted velocity, the conformal decomposition is performed, which enables the solution to capture the weak discontinuity in the velocity and strong discontinuity in the pressure. In order to get an updated solution on the now updated mesh, the momentum equation is solved again to obtain $\mathbf{u}^{n+1}$. To get second-order temporal accuracy, the BDF2 time integrator is used for both the level set and momentum equations.

The notable differences between the predictor and corrector are the domains of integration, the moving mesh term in the corrector, and the fact that the semi-implicit term in the corrector is based on the velocity correction instead of the full velocity field. For all Navier-Stokes solves, PSPG and SUPG stabilization are employed.

Sharp Interface Conditions for Dynamic Wetting

CDFEM allows for the boundary conditions to be applied in a sharp manner along the wetting line where the fluid interface meets the domain boundary. Two types of boundary conditions are combined to provide accurate wetting behavior. First, a sharp version of the Navier slip condition is applied all along the wall to capture behavior that transitions from wetting line motion to no-slip like behavior away form the wetting line. Second, a traction boundary condition pulling at the equilibrium contact angle captures the fine scale effect of wetting that cannot be captured well with reasonable mesh sizes.

Navier-Slip Condition for Momentum.

The Navier-Slip boundary condition imposes a traction on the fluid proportional to the difference between the fluid velocity and the wall velocity. This boundary condition is attractive in dynamic wetting applications where the no-slip condition must be relaxed to allow the wetting line to move along the wall [18] [4]. Using consistent finite element integration, the contribution to the momentum equation for the Navier-slip condition is given as

$$\int_{\Gamma_w^{n+1}} \frac{\mu}{\beta^*} \left(\mathbf{u}_w - \mathbf{u}^{n+1}\right) \cdot \mathbf{w}_i \mathrm{d}\Gamma, \tag{2}$$

where Γ_w is used to denote wall boundary of the fluid, $\mathbf{u}_w$ is the wall velocity, and β^* is the slip length describing the strength of the resistance to flow along the wall. This must be determined from experiments. Along the lines of [13] we can recast this equation to use a proportionality constant that depends inversely

on the mesh size Δx. In this way, the the Navier-Slip condition can be viewed as a weakly imposed condition that approaches the no-slip condition as the mesh is refined. This equation can be recast as

$$\int_{\Gamma_w^{n+1}} \frac{\mu\beta}{\Delta x} \left(\mathbf{u}_w - \mathbf{u}^{n+1}\right) \cdot \mathbf{w}_i \mathrm{d}\Gamma, \tag{3}$$

where we replace the slip length β^* with the non-dimensional slip coefficient $\beta = \Delta x/\beta^*$. Often implementations will take care to apply this condition only in the tangent directions to the wall. However, the normal velocity is normally set to zero using a Dirichlet condition, removing the normal contribution to the momentum equation. So here the slip condition is applied as a vector, since only tangent components will remain anyway.

Sharp Interface Traction Condition for Dynamic Wetting.

The Laplace-Beltrami form for surface tension incorporates an edge term where the fluid interface meets the external boundary. As described in [13] this term can be used to weakly specify the equilibrium contact angle. This accomplished by assembling an additional term in the momentum equation by integrating along the contact line,

$$\int_{\zeta^{n+1}} \sigma \left(\cos(\theta_s)\mathbf{t}_w + \sin(\theta_s)\mathbf{n}_w\right) \cdot \mathbf{w}_i \mathrm{d}\Gamma, \tag{4}$$

where ζ is the contact line and $\mathbf{t}_w$ is the tangent to the wall oriented in the direction of fluid interface normal,$\mathbf{n}_f$ and is given by

$$\mathbf{t}_w = \frac{\mathbf{n}_f - \left(\mathbf{n}_f \cdot \mathbf{n}_w\right)\mathbf{n}_w}{\left|\mathbf{n}_f - \left(\mathbf{n}_f \cdot \mathbf{n}_w\right)\mathbf{n}_w\right|}, \tag{5}$$

where $\mathbf{n}_w$ is the wall normal. This term only weakly imposes the equilibrium contact angle. It allows the dynamic contact angle to develop as a natural balance of the forces at the wall. The only free parameter in this system of boundary conditions is the dimensionless slip coeffcient β. Just as is done for the slip condition, this traction is specified as a vector condition, rather than limiting it to the tangent direction. The normal direction is zeroed using a Dirichlet condition on the velocity component normal to the wall to enforce the no pentration conditon.

3. COMPARISON WITH EXACT SOLUTIONS

Two and three dimensional benchmark problems are used to evaluate the proposed methods. Unless otherwise specified, the second-order, semi-implicit method is used.

Two-dimensional Decay of a Capillary Wave

The damped oscillation of two immiscible viscous fluids with finite surface tension σ is simulated within the presented finite-element framework and compared with the analytical solution provided by Prosperetti [19]. Here, a small amplitude sinusoidal disturbance of wavelength $\lambda = 2\pi$ is superimposed on two fluids each occupying half of the two-dimensional computational domain and separated by a common interface with surface tension σ. The Ohnesorge number $Oh = \mu/(\sigma\rho\lambda)^{1/2} = 1/\sqrt{3000}$ and the dimensionless viscosity $\varepsilon = \mu\kappa^2/(\rho\omega_0) = 6.47\times10^{-2}$. Here, $\kappa = \lambda/2\pi$ is the wavelength and ω_0 is the frequency defined as $\omega_0 = \sqrt{(\sigma\kappa)^3/(2\rho)}$.

Based on previous studies that also examined this benchmark problem, the amplitude of the disturbance was set as $A = 0.01\lambda$ and the domain was chosen to be $[-\lambda/2,\lambda/2]\,[-\lambda/2,\lambda/2]$. The decay of the initial sinusoidal wave was simulated until a dimensionless time, $t\omega_0$, of 25. A typical numerical solution is shown along with the analytical solution [19] in figure 1. Taking advantage of the interface stabilization term in both the first-order and second-order methods, the time step is selected to be much larger the explicit capillary time step limit. Regardless, no stability issues are encountered.

Oscillation of an Ellipsoidal Bubble

To examine the accuracy of the proposed method in three dimensions, the oscillatory behavior of an axisymmetric, ellipsoidal drop is simulated. The resulting frequency of the oscillation is compared with the analytical solution reported in [20]. The frequency of the second mode for the oscillation of a droplet immersed in another fluid is given by:

$$\omega_2 = \omega_2^* - \frac{\alpha\sqrt{\omega_2^*}}{2} + \frac{\alpha^2}{4}, \tag{6}$$

where

$$\omega_2^* = \sqrt{\frac{24\sigma}{R^3\left(3\rho_i + 2\rho_o\right)}}, \tag{7}$$

and R is the radius of the drop at equilibrium, σ is the surface tension, and ρ_i, ρ_o are the densities of the innner and outer fluids, respectively. The parameter α is given by,

$$\alpha = \frac{25\sqrt{\mu_i\rho_i\mu_o\rho_o}}{\sqrt{2}R\left(3\rho_i + 2\rho_o\right)\left(\sqrt{\mu_i\rho_i} + \sqrt{\mu_o\rho_o}\right)}, \tag{8}$$

where μ_i, μ_o are the viscosities of the inner and outer fluids, respectively.

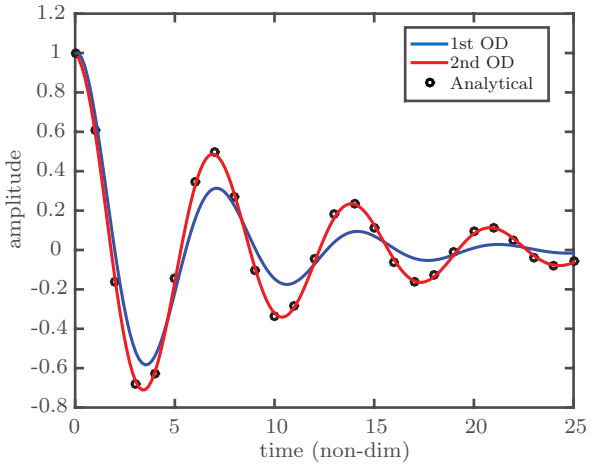

FIGURE 1. Model comparisons with analytic results of Prosperetti [19] for the sinusoidal temporal wave decay of fluid interface amplitude.

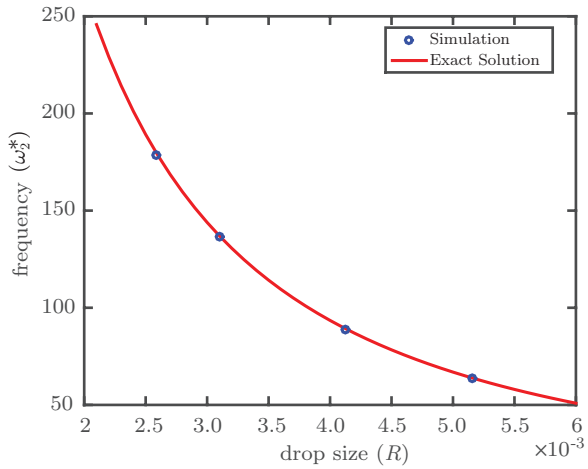

FIGURE 2. Comparison of analytical expression for the frequency of the second mode of oscillation with simulation results for the ellipsoidal drop oscillation simulation at multiple drop radii.

The behavior of an ellipsoidal drop was simulated for 1 second. The inner fluid was assigned the density, $\rho_i = 1000$, and viscosity, $\mu_i = 1 \times 10^{-3}$. The outer fluid was assigned the density, $\rho_o = 1$, and viscosity, $\mu_o = 1.8 \times 10^{-5}$. The surface tension was specified as $\sigma = 0.07$. Multiple drop sizes were simulated using the proposed second-order accurate scheme, and the resulting frequency of oscillation was compared to the analytical solution. The semi-axes of the initial ellipsoidal drop were initialized as $[1.1 \times R, R, R]$. As the simulation progressed, the length of the drop in the x-direction was computed. To compute the simulation frequency, this length versus time was fit to a decaying exponential of the form, $L_x(t) = Ae^{-Bt}\cos(\omega t + D) + C$. A commercial software program (MATLAB R2016a, The MathWorks Inc., Natick, MA) was used to fit the exponential to determine the constants A, B, C, D, ω. Figure 2 shows the analytical expression for the frequency of the second mode of oscillation along with the simulation results for drop sizes of $R = 2.5 \times 10^{-3}, 3 \times 10^{-3}, 4 \times 10^{-3}, 5 \times 10^{-3}$. These simulations were performed on a cubed domain of size 0.02, and the no-stress boundary conditions were applied at the domain boundaries. This time step is nearly twice the explicit time step size given in Eqn. 1, but again there are no stability issues by virtue of the semi-implicit algorithm. Given the relatively coarse mesh size and time step, the agreement is very good for all drop sizes.

TABLE 1. Properties of the various fluids used in the capillary injection simulations, the surface tension σ and static contact angle θ_s are assumed with air as the non-wetting fluid.

Wetting Fluid	ρ (kg/m^3)	μ (Pa$\cdot$s)	σ (N/m)	θ_s
Water	997	0.0011	0.073	6°
Santicizer 405	1130	11.2	0.043	67°
Admex 760	1150	109.3	0.043	69°

4. VALIDATION FOR DYNAMIC WETTING APPLICATIONS

Here we will compare our model with moving meniscus experimental data [21], which elucidate the importance of an accurate representation of the dynamics near the contact line. In the experiments of Hoffman [21], one wall attached to the meniscus is moved at constant velocity and the dynamic angle is measured as a function of this velocity, often cast as a capillary number Ca. Here, we replicate the capillary number dependence on the dynamic angle reported by Hoffman [21] through a capillary injection problem, where the meniscus is advected at the bottom of the capillary tube at constant velocity.

In the subsequent section, the contact line speed V_{CL} is measured instantaneously at the exact location of the contact line and the dynamic contact angle θ_d is obtained by fitting the interface to the closest representative circle utilizing a least-squares method and using the relationship $\theta_d = \pi/2 - \sin^{-1}(r/r_f)$ where r is the radius of the capillary tube and r_f is the radius of the fitted circle to the meniscus. The model fitting is accomplished through parametrically fitting the slip coefficient β^* to the discrete data points provided in the experiments for both two-dimensional and three-dimensional simulations. While the choice of the real slip length is necessarily grid resolution dependent, we will show that once a suitable slip length is chosen, the choice of β can be accurately made for different grid resolutions. The time step is chosen adaptively such that the level-set and momentum Courant-Friedrichs-Lewy (CFL) number does not exceed 0.5. When the CFL constraint is satisfied, the maximum time step should not exceed an integer multiple of the physical capillary time scale $\Delta t_{max} \leq n \times \bar{\mu} r/\sigma$ where $\bar{\mu}$ represents the average viscosity of the wetting and non-wetting fluid.

Capillary Injection

In order to investigate the potential for our model to achieve grid independence, we take the case of Sancticizer 405 at Ca $=$ 0.044 where $\theta_d \approx 115°$ from experiment [21]. The contact angle θ_d vs. time for fixed β^* at various grid spacings Δx is shown in figure 3(a). For all grid spacings, the dynamic angle is initiated at $\theta_d = 90°$, and as the meniscus is pushed through the tube, the dynamic angle adjusts until reaching an equilibrium. This equilibrium angle changes, necessarily, since the slip length β^* is grid dependent if the Navier slip condition is cast as it is in equation 2. However, if we recast the slip condition as equation 3 and hold $\beta = \Delta x/\beta^* = 62.5$ as a constant, then the solution becomes grid independent as shown through convergence of θ_d in figure 3(b) for all resolutions; supporting the conclusions of [13].

5. CONCLUSIONS

The Conformal Decomposition Finite Element Methods (CDFEM) described here have been shown to compare well with exact solutions. Weak forms for the contact angle and no-slip conditions are shown to able to reproduce dynamic contact angle behavior. Future verification work will show the convergence of the methods through detailed comparisons with the exact solutions as well as validation through comparison of dynamic wetting behavior with experiments.

ACKNOWLEDGMENT

Work by AK and MJM was supported by the Center for Frontiers of Subsurface Energy Security, an Energy Frontier Research Center funded by DOE, Office of Science, BES under Award DE-SC0001114. Sandia National Laboratories is a multimission laboratory managed and operated by National Technology and Engineering Solutions of Sandia, LLC, a wholly owned subsidiary of Honeywell International, Inc., for the U.S. Department of Energy's National Nuclear Security Administration under contract DE-NA0003525.

REFERENCES

[1] Voinov, O., 1976. "Hydrodynamics of wetting". *Fluid Dynamics*, ***11***(5), pp. 714–721.

[2] de Gennes, P., Brochard-Wyart, F., and Quere, D., 2004. *Capillarity and wetting phenomena: Drops, Bubbles, Pearls, Waves*. Springer.

[3] Tanner, L., 1979. "The spreading of silicone oil drops on horizontal surfaces". *J. Phys. D*, ***12***, pp. 1473–1483.

[4] Cox, R. G., 1986. "The dynamics of the spreading of liquids on a solid surface. part 1. viscous flow". *Journal of Fluid Mechanics*, ***168***, 07, pp. 169–194.

[5] Blake, T., and Haynes, J., 1969. "Kinetics of liquid/liquid displacments". *Journal of Colloid and Interface Science*, ***30***, pp. 421–423.

[6] Blake, T., 2006. "The physics of moving wetting lines". *Journal of Colloid and Interface Science*, ***299***, pp. 1–13.

[7] Renardy, M., Renardy, Y., and Li, J., 2006. "Numerical simulation of moving contact line problems using a volume-of-fluid method". *Journal of Computational Physics*, ***171***, pp. 243–263.

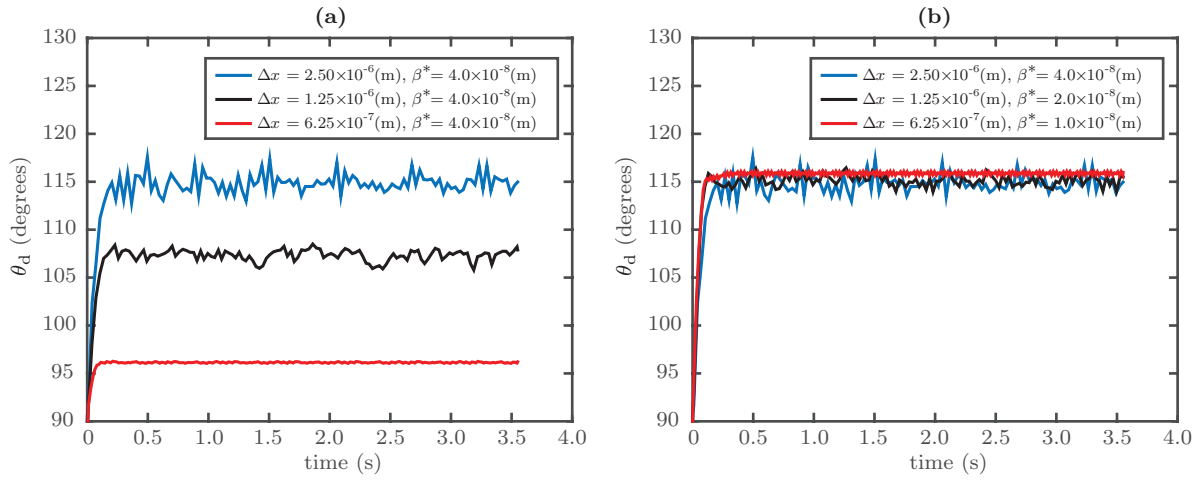

FIGURE 3. Dynamic contact angle θ_d vs. time at Ca $= 4.4 \times 10^{-2}$ at various resolutions for Santicizer 405; (a) Holding $\beta^* = 4.0 \times 10^{-8}$ m constant, (b) Holding $\beta = 62.5$ constant.

[8] Afkhami, S., Zaleski, S., and Bussmann, M., 2009. "A mesh-dependent model for applying dynamic contact angles to vof simulations". *Journal of Computational Physics*, ***228***, pp. 5370–5389.

[9] Chen, Y., Mertz, R., and Kulenovic, R., 2009. "Numerical simulation of bubble formation on orifice plates with a moving contact line". *Int. J. of Multiphase Flow*, ***35***, pp. 66–77.

[10] Sui, Y., and Spelt, P., 2013. "Validation and modification of asymptotic analysis of slow and rapid droplet spreading by numerical simulation". *J. of Fluid Mechanics*, ***715***, pp. 283–313.

[11] Jacqmin, D., 2000. "Contact-line dynamics of a diffuse fluid interface". *J. of Fluid Mechanics*, ***402***, pp. 57–88.

[12] Sprittles, J., and Shikhmurzaev, Y., 2012. "Finite element framework for describing dynamic wetting phenomena". *Int. J. Num. Meth. Fluids*, ***68***, pp. 1257–1298.

[13] Ganesan, S., Rajasekaran, S., and Tobiska, L., 2014. "Numerical modeling of the non-isothermal liquid droplet impact on a hot solid substrate". *International Journal of Heat and Mass Transfer*, ***78***, pp. 670 – 687.

[14] Kramer, R. M. J., and Noble, D. R., 2014. "A conformal decomposition finite element method for arbitrary discontinuities on moving interfaces". *International Journal for Numerical Methods in Engineering*, ***100***(2), pp. 87–110.

[15] Noble, D. R., Newren, E. P., and Lechman, J. B., 2010. "A conformal decomposition finite element method for modeling stationary fluid interface problems". *International Journal for Numerical Methods in Fluids*, ***63***(6), pp. 725–742.

[16] Hysing, S., 2006. "A new implicit surface tension implementation for interfacial flows". *International Journal for Numerical Methods in Fluids*, ***51***(6), pp. 659–672.

[17] Denner, F., Evrard, F., Serfaty, R., and van Wachem, B. G., 2017. "Artificial viscosity model to mitigate numerical artifacts at fluid interfaces with surface tension". *Computers & Fluids*, ***143***, pp. 59 – 72.

[18] V., E. B. D., 1976. "The moving contact line: the slip boundary condition". *Journal of Fluid Mechanics*, ***77***(4), 10, pp. 665–684.

[19] Prosperetti, A., 1981. "Motion of two superposed viscous fluids". *The Physics of Fluids*, ***24***(7), pp. 1217–1223.

[20] Miller, C. A., and Scriven, L. E., 1968. "The oscillations of a fluid droplet immersed in another fluid". *Journal of Fluid Mechanics*, ***32***, pp. 417–435.

[21] Hoffman, R. L., 1975. "A study of the advancing interface. I. interface shape in liquid-gas systems". *Journal of colloid and interface science*, ***50***(2), pp. 228–241.